ORIGINAL ARTICLE

Recurrent Processing of Contour Integration in the Human Visual Cortex as Revealed By fMRI-Guided TMS

Ya Li[1], Yonghui Wang[1] and Sheng Li[2,3,4,5]

[1]School of Psychology, Shaanxi Normal University, Xi'an 710062, China, [2]School of Psychological and Cognitive Sciences, Peking University, Beijing 100871, China, [3]Beijing Key Laboratory of Behavior and Mental Health, Peking University, Beijing 100871, China, [4]PKU-IDG/McGovern Institute for Brain Research, Peking University, Beijing 100871, China and [5]Key Laboratory of Machine Perception (Ministry of Education), Peking University, Beijing 100871, China

Address correspondence to Sheng Li, School of Psychological and Cognitive Sciences, Peking University, 5 Yiheyuan Road, Haidian, Beijing 100871, China. Email: sli@pku.edu.cn

Abstract

Contour integration is a critical step in visual perception because it groups discretely local elements into perceptually global contours. Previous investigations have suggested that striate and extrastriate visual areas are involved in this mid-level processing of visual perception. However, the temporal dynamics of these areas in the human brain during contour integration is less understood. The present study used functional magnetic resonance imaging-guided transcranial magnetic stimulation (TMS) to briefly disrupt 1 of 2 visual areas (V1/V2 and V3B) and examined the causal contributions of these areas to contour detection. The results demonstrated that the earliest critical time window at which behavioral detection performance was impaired by TMS pluses differed between V1/V2 and V3B. The first critical window of V3B (90–110 ms after stimulus onset) was earlier than that of V1/V2 (120–140 ms after stimulus onset), thus indicating that feedback connection from higher to lower area was necessary for complete contour integration. These results suggested that the fine processing of contour-related information in V1/V2 follows the generation of a coarse template in the higher visual areas, such as V3B. Our findings provide direct causal evidence that a recurrent mechanism is necessary for the integration of contours from cluttered background in the human brain.

Key words: feedback connection, perceptual grouping, primary visual cortex, transcranial magnetic stimulation, V3B

Introduction

The human visual system efficiently extracts local elements from cluttered backgrounds and integrates these elements into meaningful contour perception. This process is a critical step before object recognition, in which contours often play an important role in defining the shapes and borders of the to be recognized objects. Previous behavioral investigations have suggested that contour integration follows the Gestalt rule of good continuation because the neighboring elements are integrated if they satisfy the joint constraints of position and orientation along a smooth contour (Field et al. 1993; see reviews, Hess et al. 2003). This proposal is consistent with the morphology of horizontal connections in V1, which exhibit the strongest connections between neurons with a similar orientation preference (Bosking et al. 1997; Stettler et al. 2002). Neurophysiological studies in monkeys have further demonstrated that the responses of

individual neurons in V1 encode contour information and correlate with behavior performance (Kapadia et al. 1995; Li et al. 2006).

However, contour integration is difficult to implement via a V1-initiated feed-forward mechanism alone. V1 represents the world fragmentally at the initial stage of visual processing. Higher-level areas, such as V4, integrate information from V1 over a larger area of the visual field and represent more complex shapes. However, the challenge of disambiguating the local elements that belong to the contour and background remains even for higher-level areas with large receptive fields. A recurrent mechanism with various implementations may meet this challenge (Angelucci et al. 2002; Foxe and Simpson 2002; Kourtzi et al. 2003; Li et al. 2006, 2008; Jehee et al. 2007; Ramalingam et al. 2013; Shpaner et al. 2013; Mijovi et al. 2014; Drewes et al. 2016). Feed-forward processing may create a coarse template in higher visual areas followed by a feedback sweep to guide the fine processing of contour-related information in lower visual areas (Roelfsema 2006; Epshtein et al. 2008; Roelfsema and Houtkamp 2011).

Furthermore, the involvements of striate and extrastriate cortical areas in contour integration has been observed in the human brain by using the functional magnetic resonance imaging (fMRI) technique (Altmann et al. 2003; Kourtzi et al. 2003; Kuai et al. 2016). However, with this technique, it is difficult to infer the temporal dynamics between the processing of V1 and higher visual areas because of the temporal resolution limitations. Chen and colleagues (2014) have simultaneously recorded neural activities in V1 and V4 areas in monkeys and have found that the onset latency of contour-related responses in V4 appears earlier than those in V1, thus indicating that the contour-related activities observed in V1 in early studies were probably driven by feedback signals from V4. However, to establish a causal relationship, the contour integration process must be disrupted by interfering with V4 activity before it sends the contour-related signals back to V1. Transcranial magnetic stimulation (TMS), as a noninvasive tool to stimulate specific cortical regions, may be used to address this issue in the human brain.

The present study used fMRI-guided TMS to disrupt the lower-level (V1/V2) and higher-level (V3B) visual areas and to examine the chronological order of the critical roles of these areas in contour integration while participants performed a contour detection task. V3B was chosen as the stimulation site because it is a homolog of monkey dorsal V4 in the human brain (Tootell and Hadjikhani 2001; Tootell et al. 2003), and it is associated with the processing of contour integration (Schwarzkopf et al. 2009; Zhang and Kourtzi 2010; Kuai et al. 2016) or more generally perceptual integration (Ostwald et al. 2008; Li et al. 2009; Lestou et al. 2014). The study consisted of two experiments. In Experiment 1, we disrupted V1/V2 and V3B at 4 stimulus onset asynchronies (SOAs) and the results showed that the first critical windows (i.e., SOAs) were 90–110 ms after the stimulus onset for V3B and 120–140 ms after the stimulus onset for V1/V2, respectively. In Experiment 2, we specifically examined the interaction between the 2 identified SOAs and the 2 visual areas under TMS, in order to increase the statistical power and reach a conclusive argument. The results of Experiment 2 confirmed the main findings of Experiment 1 by demonstrating that the interference effect of V3B stimulation occurred earlier than that of V1/V2. Our findings support the hypothesis that a recurrent mechanism is required in the human visual cortex for the detection of contours embedded in a cluttered background.

Materials and Methods

Experiment 1

Participants

Twenty naïve participants (10 males, 10 females; mean age = 21 years; range = 18–25 years) were recruited for the experiment. Participants were students at Peking University with normal or corrected-to-normal vision. All participants except one were right-handed, and all participants had no known neurological or visual disorders. Participants provided written informed consent before the experiment. The local ethics committee approved the study.

Stimuli and Aperture

Stimuli were displayed on a gray uniform background of a CRT monitor with a refresh rate of 100 Hz. The stimuli and procedures were programmed with Psychtoolbox 3 (Brainard 1997; Pelli 1997; Kleiner et al. 2007) in a MATLAB (Mathworks, Natrick, MA) programming environment. Stimuli for the contour detection task were Gabor fields (12.66° × 12.66°) that consisted of randomly distributed and oriented Gabor elements (peak spatial frequency: 6.62 cycles/degree, envelope σ: 0.10°, contrast: 100%). A contour was embedded in the Gabor field. The contour consisted of 11 Gabor elements and was presented in the upper left (ipsilateral to the side of TMS) or lower right visual field (contralateral to the side of TMS) (see Fig. 1 and Fig. S1A). The orientations of the Gabor elements of the contour were deviated relative to the underlying path of the contour to avoid floor or ceiling performance. The orientation deviation was determined individually for each participant in a practice phase before the main experiment to ensure that the behavioral task was performed at an intermediate level of difficulty. The Gabor fields were generated using an iterative procedure to ensure a minimum inter-element separation of 0.86°. Participants were required to fixate on a small red dot in the center of the screen throughout the experiment.

Procedure

Experiment 1 consisted of 3 sessions: an fMRI session and 2 TMS sessions. We used the population receptive field (pRF) model (Dumoulin and Wandell 2008; Wandell and Winawer 2015) in the fMRI session to precisely map the participants' retinotopic areas and the regions in V1 and V3B that corresponded to the visual field that the contour presented. The coordinates of the defined V1 and V3B areas were used in the TMS sessions to examine the behavioral effects when the magnetic pulses interrupted these regions during the contour detection task.

fMRI Session

Identifying the stimulation site (V1 and V3B) with the pRF model had three advantages. First, the pRF parameters can be well estimated for individual participants. Second, the pRF parameters can be estimated in the stimulus coordinate system, thus providing a direct link between the stimulus locations during the fMRI and TMS sessions. Third, the target regions defined by pRF are more objective than multifocal fMRI, which determines the stimulus location on the basis of the experimenter-defined general linear model (GLM) threshold (Vanni et al. 2005). Additionally, we had sixteen participants performed a contour detection task inside the scanner and to further constrained the stimulation sites to those voxels that responded more to the Gabor field than the fixation condition. For these participants, we determined the center of the
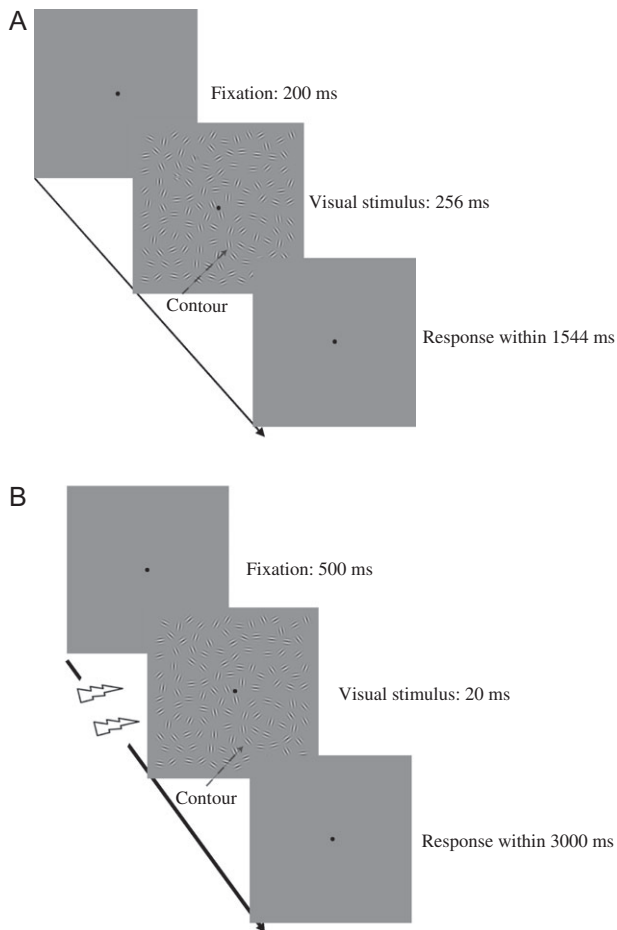
Figure 1. Experimental procedures. (*A*) An example trial of the contour detection task in the fMRI session. (*B*) An example trial of the contour detection task in the TMS sessions. Each element of the contour stimuli was magnified for better demonstration purposes only. Double-pulse TMS was applied at different SOAs with respect to the onset of the contour stimulus while participants performed a contour detection task. Specifically, double-pulse TMS was delivered over the dorsal V1/V2 and V3B of the left hemisphere at 4 different SOAs (60/80, 90/110, 120/140 and 150/170 ms) (plus a no-TMS baseline condition) in Experiments 1 and 2 different SOAs (90/110 ms and 120/140 ms) (plus a no-TMS baseline condition) in Experiment 2.

stimulation sites as a conjunction of 2 sets of voxels: (1) the voxels with pRFs that were located in the stimulus-presented quadrant of the visual field and (2) the voxels that responded more to the Gabor field than the fixation condition. The stimulation sites in the other four participants were determined solely on the basis of the pRF method.

Data acquisition: Imaging data were collected with a 3T Siemens Prisma scanner equipped with a 20-channel receiver head coil. Functional data were acquired with a gradient-echo EPI sequence (TR = 2000 ms, TE = 30 ms, FOV = 152 × 152 mm^2, matrix size: 76 × 76, flip angle: 90°, gap = 0 mm; number of slices: 28, slice thickness: 2.5 mm, slice orientation: transversal). A high-resolution T1-weighted three-dimensional anatomical data set was collected to aid in registration (MPRAGE, TR = 2530 ms, TE = 2.98 ms, FOV = 256 × 224 mm^2, flip angle: 7°, resolution: 0.5 × 0.5 × 1 mm^3, number of slices: 192, slice thickness: 1 mm, slice orientation: sagittal).

pRF mapping task: The borders of retinotopic visual areas (V1, V2, V3, and V3B) and the pRF of each voxel were mapped for

each participant with the pRF method. There were 5 functional runs: 1 run to estimate the hemodynamic response function (HRF), and 4 runs for pRF mapping. We used a flickering high-contrast checkerboard pattern (100% contrast) for both measurements to maximize the visual response (Fig. S1B). The run for estimating the HRF consisted of 8 blocks and lasted for 308 s. A flickering checkered disc (10.35°, 100% contrast) was presented for 4 s, and this was followed by a 32 s blank interval in each block. Each run for pRF mapping consisted of 8 blocks of bar stimuli and 4 blank blocks. Each block lasted for 36 s. A bar (width: 2.14°) passed through an invisible circular aperture (radius: 10.22°) in 18 steps (step size: 1.07°) in each block with bar stimuli. These bar apertures moved along one of four orientations (0°, 45°, 90°, and 135°) in two opposing directions. An 8-s blank interval was presented at the beginning, and a 12-s blank interval was presented at the end of each HRF estimation and pRF mapping run. Participants were asked to maintain fixation and press the right button as soon as possible whenever a green fixation appeared.

Contour detection task: To identify the voxels that were more responsive during the contour detection task, we conducted 4 event-related runs. Each run consisted of 81 trials (each lasted for 2 s), and blank intervals were presented at the beginning (8 s) and end (12 s) of the run. The order of the conditions (contour present, contour absent, and fixation) was counterbalanced by using M-sequence (Buracas and Boynton 2002). As shown in Figure 1A, each trial began with a 200 ms fixation, and this was followed by a Gabor field with or without a contour embedded. The Gabor field stimulus was presented for 256 ms and the embedded contour was presented in only the lower right visual field. Participants were required to maintain fixation and indicate whether the contour was present. They were asked to respond as quickly and accurately as possible. No feedback was provided after each trial.

TMS Sessions

The 2 TMS sessions were separated by at least 3 days. The order of the V1/V2 and V3B stimulations was counterbalanced between participants. We used the term V1/V2, instead of V1 alone, in the TMS sessions because the folded anatomical structure of the visual cortex and the spatial resolution of TMS made it very likely that we would also stimulate a small part of V2 with the targeted V1 area (Koivisto et al. 2011; Silvanto, Lavie et al. 2005; Salminen-Vaparanta et al. 2012). However, V1 probably contributed most of the behavioral effects observed, given the critical role of V1 in contour integration revealed in previous neurophysiological studies (Kapadia et al. 1995; Li et al. 2006; Chen et al. 2014).

TMS protocol: TMS pulses were delivered through a MagStim Super Rapid^2 stimulator (MagStim Company) in combination with a 70-mm figure-of-8 coil (Fig. 2A). The head position of each participant was co-registered, and the specific locations of the stimulation sites (dorsal V1/V2 and V3B at left hemisphere) were localized using the fMRI-guided Visor navigation system (Visor2; Advanced Neuro Technology, Enschede, The Netherlands) on the basis of the mapping results from the fMRI session. The center of the coil was placed tangentially over the stimulation site and kept steady in that position on the scalp with a mechanical arm. During the stimulation, the coil was held with the handle pointing upwards and its position was real-time monitored using Visor2 throughout each session. The intensity of the TMS pulses was set to 60% of the maximum strength for all participants, and none of the participants
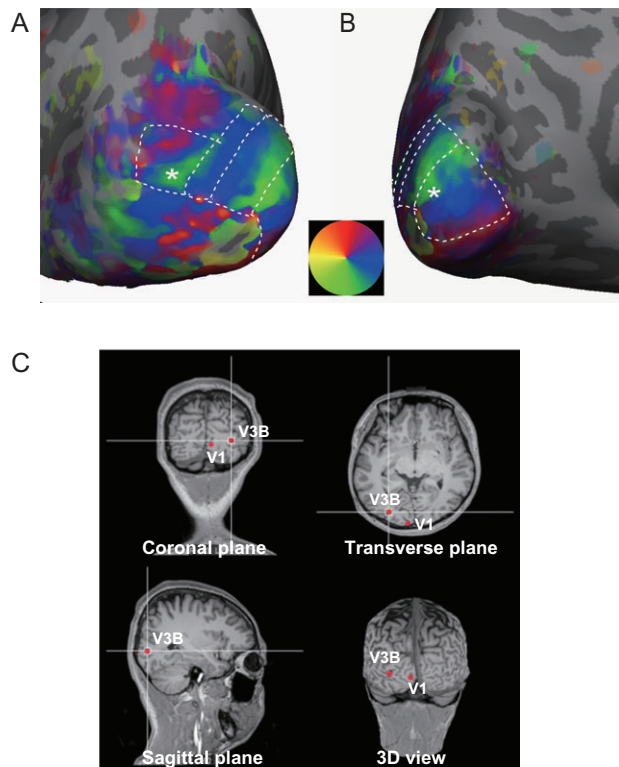
Figure 2. Illustrations of the TMS stimulation sites. The stimulation sites are marked with white asterisk on top of retinotopic maps for (A) V3B and (B) V1. In both (A) and (B), polar angle maps of one representative participant were overlaid on the left inflated cortical surface. The color corresponds to the visual field representation, as indicated by the color wheel in the middle of the figure. The white dash lines indicate the boundaries between V1, V2, V3, and V3B. (C) TMS coil locations for V1/V2 and V3B stimulation on the MRI anatomical images of one representative participant.

reported phosphenes during the experiment (Silvanto, Lavie et al. 2005; Pitcher et al. 2012). Double-pulse TMS was applied at four SOA conditions (60/80 ms, 90/110 ms, 120/140 ms, and 150/170 ms after the stimulus onset) over the dorsal V1/V2 and V3B regions of the left hemisphere. A double-pulse of TMS was delivered to induce a larger inference effect than single-pulse TMS and to take advantage of the summation nature of the TMS pulses (Walsh and Pascual-Leone 2003; Silvanto, Lavie et al. 2005) while maintaining the high temporal resolution defined by the temporal interval between the two pulses (Walsh and Pascual-Leone 2003). A baseline condition was also included, in which no-TMS was applied after the stimulus onset.

Contour detection task with TMS: For half of the participants, the first TMS session began with three blocks of V1/V2 stimulation and then three blocks of V3B stimulation. An inverse order of stimulation sites was used in the second TMS session. The first and second TMS sessions for the other half of the participants began with V3B and V1/V2 stimulations, respectively. The contour detection task consisted of experimental trials in which a contour was presented in a Gabor field, and catch trials in which no contour was embedded. There were 16 experimental trials and 2 catch trials for each of the five conditions (four SOA conditions: 60/80, 90/110, 120/140, and 150/170 ms; one baseline condition: no-TMS) in each block, resulting in 96 experimental trials and 12 catch trials for each condition and each stimulation site for each participant. In half of the

experimental trials, the contour was presented in the lower right visual field, which corresponded to the stimulation sites at the left dorsal visual areas. The contour was presented in the upper left visual field in the other half of the experimental trials, which corresponded to the cortical site that was not stimulated with TMS. As shown in Figure 1B, each trial began with a 500 ms fixation period, which was followed by presentation of the Gabor field for 20 ms. The background remained gray until a response occurred or 3 s had elapsed. Participants were required to maintain fixation and indicate whether the contour was presented in the upper left or lower right visual field in both types of trials as quickly and accurately as possible. No feedback was provided.

Data Analysis: All behavioral indices (i.e., accuracy, RTs, and inverse efficiency) were analyzed with 2-way repeated measures analyses of variance (ANOVA), with stimulation site and SOA as within-subject factors. For each participant, we excluded the trials whose RTs were beyond 3 SDs from the mean RTs of all correct trials. Inverse efficiency (i.e., RT divided by proportion correct) of the correct trials were used to account for the possible trade-off between speed and accuracy (Mevorach et al. 2006, 2009; Brozzoli et al. 2008; Pasalar et al. 2010; Bardi et al. 2012; Bona et al. 2014). All behavioral indices were then normalized for each stimulation site by subtracting the baseline condition (no-TMS) from the TMS conditions at each SOA. Moreover, TMS effects were calculated as the difference in the normalized index values between the trials, in which the contour was located in the contralateral relative to ipsilateral visual field to the TMS site. The trials with ipsilateral presentation of contour stimuli were used to control for the possible unspecific TMS artifacts such as acoustic noise, somatosensory stimulation, and coil position.

Moreover, one-sample *t*-test (one-tail, compared with 0) was performed to examine the TMS interference effect at different SOAs, and more importantly, to identify critical SOAs for the two stimulation sites. To identifying candidates for further hypothesis testing, we used FDR method to adjust the threshold of significance for the multiple homogeneous comparisons of one-sample *t*-tests, as Bonferroni correction could be too stringent for eight comparisons.

Experiment 2

Participants

Twenty naïve participants (11 males, 9 females; range = 20–26 years) were recruited for the experiment, and 8 of these subjects had participated in Experiment 1. Participants were students at Peking University and had normal or corrected-to-normal vision. All participants except one were right-handed, and no participants had known neurological or visual disorders. Participants provided written informed consent before the experiment. The local ethics committee approved the study.

Stimuli and Aperture

The stimuli in Experiment 2 were the same as those in Experiment 1, with the exception that the Gabor orientation deviation of the contours in the TMS sessions was predetermined in the additional psychophysics session. Moreover, to equate the task difficulty of contour detection between contralateral and ipsilateral visual field, the Gabor orientation deviation was estimated separately for the 2 visual fields by using the staircase method.

Procedure

The general procedure in Experiment 2 was identical to that in Experiment 1, except that a psychophysics session was performed before the fMRI session. The detection thresholds of the left and right visual fields of each participant were measured separately in the psychophysics session, for a performance level of 84% accuracy. The process of the TMS session was also identical to that in Experiment 1, except that the two TMS sessions were separated by at least one day, and there were four blocks in each session, with two blocks for each stimulation site.

Psychophysics Session

The detection thresholds of each participant of Gabor orientation deviation were estimated by using a 1-down 4-up staircase procedure in the psychophysics session, which converged at a performance level of 84% accuracy. The step size was 5° until the first wrong response occurred, after which the step size was changed to 2°. Each participant completed two staircase blocks. Each block mixed two staircases with one staircase for each contour condition (i.e., left and right visual fields). Each staircase consisted of 7 preliminary reversals and 7 experimental reversals. The geometric mean of the experimental reversals was taken as the threshold for each staircase run. The estimated 84% threshold was further confirmed in at least one more block. Each block had 40 experiment trials for each contour condition (lower left and upper right visual fields). Eye movements in the psychophysics session were measured with Eyelink 1000 plus (SR Research Ltd., Osgoode) eye-tracking device to monitor gaze position during stimulus presentation. Prior to each block, each participant's gaze was determined via a calibration process. Drift correction procedure was performed before each trial. Participants were asked to look at a red fixation dot at the center of a gray screen. The contour stimuli were not presented until the calculated gaze position fell within the square of 1° wide around the central fixation for at least 200 ms. The calibration process was repeated if the calculated gaze position was not at the center of the screen for more than 15 s before the trial started.

fMRI Session

The fMRI session in Experiment 2 was identical to that in Experiment 1.

TMS Sessions

The TMS sessions in Experiment 2 were identical to those in Experiment 1 with three exceptions. First, the Gabor stimuli used in Experiment 2 were matched in task difficulty and predetermined in the psychophysics session. Second, eye movements were monitored as described in the psychophysics session. Third, there were two SOAs (90/110 and 120/140 ms) with 96 experimental trials for each SOA condition and each stimulation site (V1/V2 and V3B).

Data Analysis: The TMS interference effect was analyzed using 2-way repeated measures ANOVA with stimulation site (V1/V2 and V3B) and SOA (90/110 and 120/140 ms) as within-subject factors. Simple effect analyses were conducted when the interaction was significant. Furthermore, one-sample t-test (one-tail, compared with 0) was performed to examine whether the TMS interference effect occurred at each SOA and each stimulation site. Multiple comparisons were corrected for simple effects and one-sample t-test by using the Bonferroni method to adjust the threshold of significance.

fMRI Data Analysis

Data preprocessing: The anatomical images were resampled to a 1-mm^3 resolution. Images were automatically segmented, and the cortical surface was reconstructed with FreeSurfer (Dale et al. 1999; Fischl et al. 1999). The first 4 functional images in each run were discarded to allow the signal to reach saturation. The remaining functional images were analyzed with SPM8 (Wellcome Trust Centre for Neuroimaging, University College London). Preprocessing of the data included realignment, slice-time correction, and three-dimensional motion correction. The processed functional data were co-registered to the high-resolution anatomical images. The volume-based functional data were projected onto the inflated cortical surface in FreeSurfer by using a custom toolbox (de Haas et al. 2014; Schwarzkopf et al. 2014; Alvarez et al. 2015) to create the surface-based data. This surface-based functional time series for each vertex were linear-trend removed, and z-scores were normalized for each run. These preprocessed surface-based data were used in all subsequent fMRI data analyses.

pRF and GLM analyses: We estimated the pRF parameters on the basis of the method proposed by Dumoulin and Wandell (2008). The pRF analysis was performed using a custom toolbox developed in the MATLAB programming environment (Schwarzkopf et al. 2014; Alvarez et al. 2015) and was restricted to a mask that covered the occipital cortex. The key pRF parameters of each vertex were fitted in a two-stage procedure for each vertex, a coarse fitting and a fine fitting (Schwarzkopf et al. 2014, see online Supplementary Material for the details of the fitting). Based on the fitted pRF parameters, the center coordinates of the vertices were transformed into polar angles and eccentricity values. The polar angles and eccentricity values were projected onto the surface shown in FreeSurfer and were used to identify the regions that represented the stimuli on the lower right visual field and to delineate the boundary of the retinotopic visual areas. The border of the early retinotopic visual areas (V1, V2, V3) was delineated according to standard procedures based on meridian mirror reversals of polar angle (Wandell et al. 2007). V3B were defined as the areas that contained a full hemifield representation of the contralateral visual field and anterior and superior to dorsal V3. The boundary between V3A and V3B was defined as the convergence of the visual fields. The approximate localization of 1–5° eccentricity and −80 to −10° polar angle relative to the horizontal meridian verified that the voxels represented stimuli in the lower right visual field. A GLM was applied to the fMRI data from the contour detection task. Vertices in V1 and V3B that exhibited significantly stronger responses to the Gabor field than fixation were identified. Finally, the defined target vertices were converted back to volume-based data to allow for compatibility with Visor2 for the TMS sessions.

Results

Experiment 1

In Experiment 1, we stimulated the dorsal left V1/V2 and V3B at four SOA conditions (60/80, 90/110, 120/140, and 150/170 ms) (plus a no-TMS as baseline condition) when the participants performed the contour detection task. The mean accuracy under the no-TMS condition was 85.7 ± 5.8%, thus indicating that the task difficulty was at an intermediate level. We calculated the interference effects for accuracy, RTs, and inverse efficiency separately (Fig. 3). Based on our definitions, a negative value of the interference effect on accuracy or a positive value
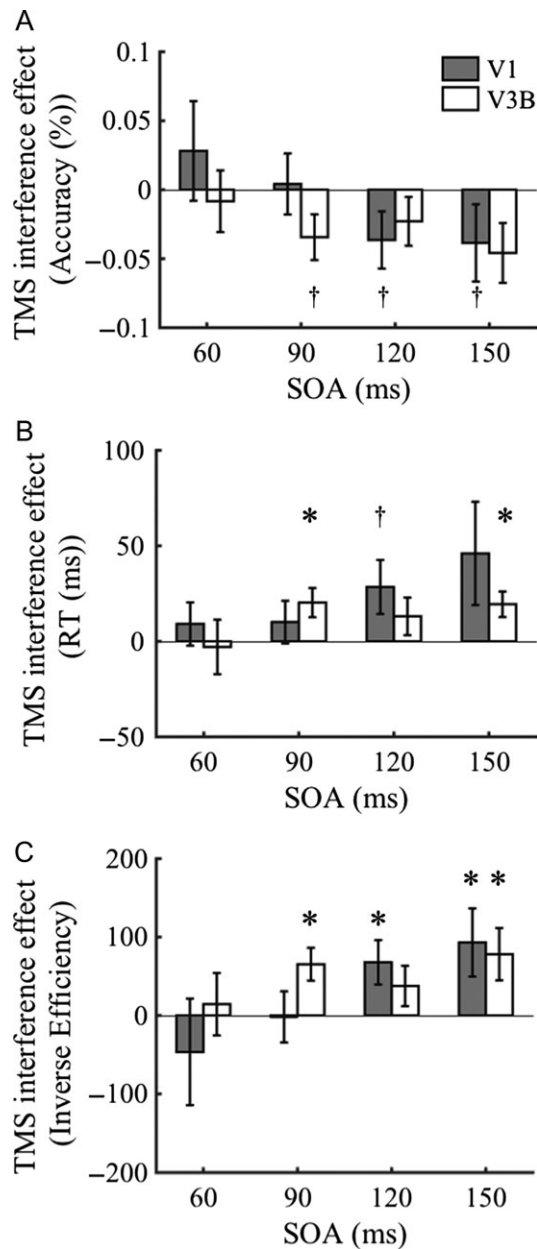
Figure 3. TMS interference effects as the function of SOAs at V1/V2 and V3B for Experiment 1 for (A) accuracy, (B) RTs, and (C) inverse efficiency. Negative value of accuracy or positive value of RTs or inverse efficiency represents an interference effect due to TMS stimulation. Error bars represent standard error of mean. The asterisks indicate the time windows in which the TMS interference effect was significantly smaller than zero for accuracy or larger than zero for RTs and inverse efficiency indicated by one-sample *t*-tests (**P <0.01 FRD corrected; *P <0.05 FRD corrected; †P <0.05 uncorrected).

of the interference effect on RTs or inverse efficiency indicates impaired contour integration when stimulating an area at a specific SOA.

We first entered the interference effects of accuracy, RTs, and inverse efficiency into separate 2-way (stimulation site × SOA) repeated measures ANOVAs. The ANOVA on accuracy revealed a significant main effect of SOA ($F(3,57)$ = 2.93, $P < 0.05$, $\eta_p^2 = 0.13$). Post hoc tests only revealed a trend of significant difference between the 60/80 ms and 150/170 ms SOA conditions ($P = 0.03$, Bonferroni-corrected threshold = 0.0083). The main

effect on stimulation site ($F(1,19) = 0.64$, $P = 0.42$, $\eta_p^2 = 0.03$) and the interaction effect ($F(3,57) = 0.83$, $P = 0.48$, $\eta_p^2 = 0.04$) were not significant. The ANOVA on RTs revealed no significant effect (Ps >0.1). Furthermore, the ANOVA on inverse efficiency showed a significant main effect of SOA ($F(3,57) = 3.22$, $P <0.05$, $\eta_p^2=0.15$). The main effect on stimulation site ($F(1,19) = 0.42$, $P = 0.52$, $\eta_p^2=0.02$) and the interaction effect ($F(3,57) = 1.19$, $P = 0.31$, $\eta_p^2=0.06$) were not significant. Post hoc tests only revealed a trend of significant difference between the 60/80 and 90/110 ms SOA conditions ($P = 0.05$, Bonferroni-corrected threshold = 0.0083).

To elucidate the critical time windows of the interference effects for V1/V2 and V3B, we further conducted one-sample *t*-tests on accuracy (FDR-corrected threshold = 0.00625), RTs (FDR-corrected threshold = 0.01875), and inverse efficiency (FDR-corrected threshold = 0.025) at each SOA and each stimulation site. The results from the three indices showed similar patterns of significance (Fig. 3). For V1/V2, we observed significant interference effects or trends of significance at 120/140 ms SOA on accuracy ($t(19) = −1.76$, $P = 0.05$, Cohen's $d = −0.39$), RTs ($t(19) = 2.02$, $P = 0.03$, Cohen's $d = 0.45$), and inverse efficiency ($t(19) = 2.40$, $P = 0.01$, Cohen's $d = 0.54$). For V3B, we observed significant interference effects or trends of significance at 90/110 ms SOA on accuracy ($t(19) = −2.07$, $P =0.03$, Cohen's $d = −0.46$), RTs ($t(19) = 2.66$, $P = 0.008$, Cohen's $d = 0.60$), and inverse efficiency ($t(19) = 3.18$, $P =0.002$, Cohen's $d = 0.71$). These results indicated that 120/140 and 90/110 ms were the most probable critical windows for V1/V2 and V3B respectively. Additionally, we also observed a trend of significance at 120/140 ms SOA for V3B on inverse efficiency ($t(19) = 1.46$, $P =0.08$, Cohen's $d = 0.33$). However, it was difficult to make inference about the role of the 120/140 ms time window for V3B given the small effect size.

Furthermore, we also observed significant effects or trends of significance at the later 150/170 ms SOA for both V1/V2 (accuracy: $t(19) = −1.38$, $P =0.09$, Cohen's $d = −0.31$; RTs: $t(19) = 1.70$, $P = 0.05$, Cohen's $d = −0.38$; inverse efficiency: $t(19) = 2.17$, $P = 0.02$, Cohen's $d = 0.49$) and V3B (accuracy: $t(19) = −2.12$, $P = 0.02$, Cohen's $d = −0.47$; RTs: $t(19) = 2.91$, $P = 0.004$, Cohen's $d = 0.65$; inverse efficiency: $t(19) = 2.37$, $P = 0.01$, Cohen's $d = 0.53$). None of other comparisons showed significant effect or trend of significance.

Based on these results, in Experiment 2, we only examined the 2 critical SOAs (90/110 and 120/140 ms) for V1/V2 and V3B. We also matched the task difficulty for both visual fields and monitored the eye movement in the TMS sessions to increase the detection power in Experiment 2.

Experiment 2

In Experiment 2, the mean accuracy for the contour detection task under the no-TMS condition was 87.3 ± 2.8% (contralateral visual field: 89.1 ± 4.0%; ipsilateral visual field: 85 ± 5.2%) and closely matched the baseline performance in Experiment 1. Again, we calculated the interference effects for accuracy, RTs, and inverse efficiency separately as shown in Figure 4.

As in Experiment 1, we entered the interference effects of accuracy, RTs, and inverse efficiency into separate 2-way (stimulation site × SOA) repeated measures ANOVAs. We hypothesized that, if the TMS stimulation disrupted the processing of contour integration, the strongest effect would be an increase in error rate (i.e., decreased accuracy). This was what we have observed from the results. The ANOVA on accuracy revealed a significant interaction effect between stimulation site and SOA ($F(1,19) = 7.37$, $P = 0.014$, $\eta_p^2=.28$). The TMS interference effects at
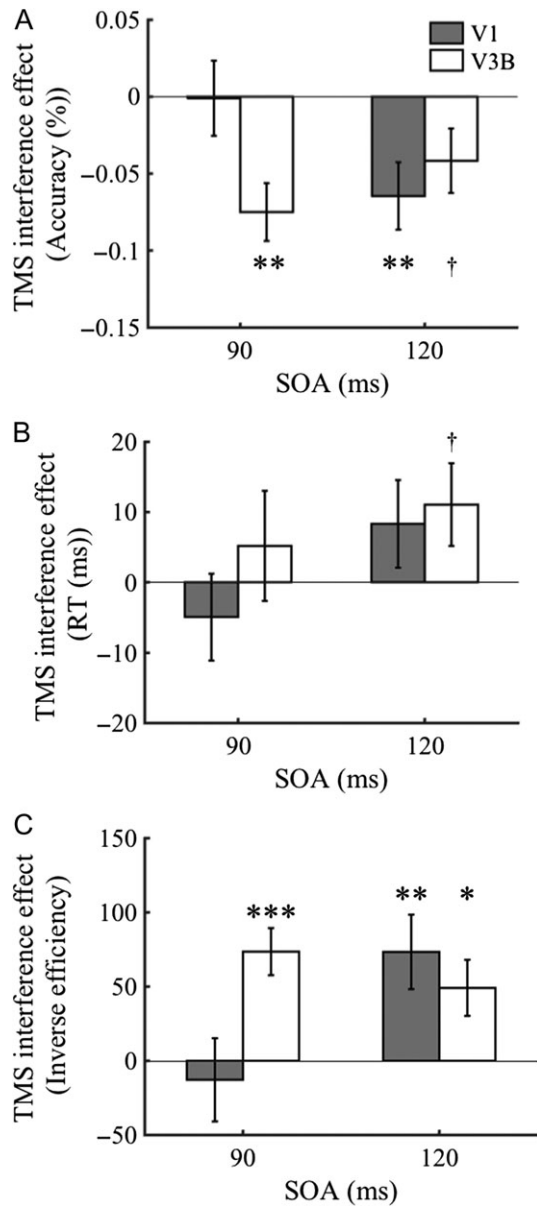
Figure 4. TMS interference effects as the function of SOAs at V1/V2 and V3B for Experiment 2 for (A) accuracy, (B) RTs, and (C) inverse efficiency. Negative value of accuracy or positive value of RTs or inverse efficiency represents an interference effect due to TMS stimulation. Error bars represent standard error of mean. The asterisks indicate the time windows in which the TMS interference effect was significantly smaller than zero for accuracy or larger than zero for RTs and inverse efficiency indicated by one-sample t-tests (***$P < 0.001$ Bonferroni-corrected; **$P < 0.01$ Bonferroni-corrected; *$P < 0.05$ Bonferroni-corrected; †$P < 0.05$ uncorrected).

the 2 stimulation sites were critically dependent on the SOA. Simple effect analysis showed that, the interference effect was larger at 120/140 ms SOA than at 90/110 ms SOA when TMS was applied over V1/V2 ($F_{(1,19)} = 6.09$, $P = 0.02$, $\eta_p^2 = .24$). In contrast, there was no significant difference between the interference effects at the 2 SOAs when TMS was applied over V3B ($F_{(1,19)} = 1.93$, $P = 0.18$, $\eta_p^2 = 0.09$). Yet, the ANOVA on RTs only revealed a trend of significance of SOA ($F_{(1,19)} = 3.24$, $P = 0.09$, $\eta_p^2 = 0.15$; all other Ps > 0.3). Furthermore, the ANOVA on inverse efficiency revealed similar pattern as on the accuracy, demonstrating a significant interaction effect between stimulation site and SOA

($F_{(1,19)} = 7.34$, $P = 0.01$, $\eta_p^2 = 0.28$). The main effects of stimulation site ($F_{(1,19)} = 2.37$, $P = .14$, $\eta_p^2 = 0.11$) and SOA ($F_{(1,19)} = 3.07$, $P = 0.10$, $\eta_p^2 = 0.14$) were not significant. Simple effect analysis showed that, when TMS was applied over V1/V2, the interference effect was larger at 120/140 ms SOA than at 90/110 ms SOA ($F_{(1,19)} = 7.67$, $P = 0.01$, $\eta_p^2 = 0.29$). In contrast, no significant difference between the interference effects at the two SOAs was observed when TMS was applied over V3B ($F_{(1,19)} = 1.23$, $P = 0.28$, $\eta_p^2 = 0.06$).

Next, we conducted one-sample t-tests (Bonferroni-corrected thresholds = 0.0125) on accuracy, RTs, and inverse efficiency to elucidate the critical time windows of the interference effects for V1/V2 and V3B. For V1/V2, we observed significant interference effects at 120/140 ms SOA on accuracy ($t(19) = -2.95$, $P = 0.004$, Cohen's $d = 0.66$) and inverse efficiency ($t(19) = 2.92$, $P = 0.004$, Cohen's $d = 0.65$). For V3B, we observed significant interference effects at 90/110 ms SOA on accuracy ($t(19) = -3.99$, $P < 0.001$, Cohen's $d = -0.89$) and inverse efficiency ($t(19) = 4.64$, $P < .001$, Cohen's $d = 1.04$). These results suggested the earliest impairments on performance due to TMS stimulation were at 120/140 ms for V1/V2 and 90/110 ms for V3B, and that the dominant form of the impairments was the increase in error rate, rather than the slowing down of the correct responses. Additionally, we also observed a trend of significance on accuracy ($t(19) = -1.99$, $P = 0.03$, Cohen's $d = -0.45$) and RTs ($t(19) = -1.88$, $P = 0.04$, Cohen's $d = 0.42$), and a significant effect on inverse efficiency ($t(19) = 2.60$, $P = 0.009$, Cohen's $d = 0.58$) at 120/140 ms SOA for V3B.

In sum, the results from Experiment 2 confirmed the main findings in Experiment 1 and suggested that the first critical time window of TMS interference for V3B was earlier than that of V1/V2, indicating an important role of recurrent processing between these two areas for contour integration.

Discussion

There is an ongoing debate regarding the contribution of higher-level visual processing to contour integration. Previous studies that directly recorded neural activities from alert animals (Kapadia et al. 1995; Li et al. 2006; Gilad et al. 2013) and pioneering behavioral investigations on human subjects (Field et al. 1993) have suggested that V1 plays a significant role in the integration process. However, other investigations have identified the critical involvement of extrastriate cortical areas in contour integration (Altmann et al. 2003; Schwarzkopf et al. 2009; Zhang and Kourtzi 2010). Notably, Chen and colleagues (2014) have simultaneously recorded V1 and V4 in monkeys and have found that the contour-related activity in V4 appears earlier than that in V1. This result provides evidence that the contour-related activities in V1 in early studies may have been driven by the recurrent processing between V1 and V4. Our results provided the first reported causal evidence of the role of the extrastriate cortex (V3B) in contour integration in the human brain. Importantly, on the basis of the chronological order of the interference effects in V1/V2 and V3B, we suggest that recurrent interactions between striate and extrastriate cortical areas play a critical role in the detection of contours embedded in a cluttered background in the human brain.

Our results demonstrated that the critical interference time window of V1/V2 follows the first critical time window for V3B. The application of double-pulse TMS over V3B at 90/110 ms after stimulus onset decreased the performance in the contour detection task, whereas the earliest time window in which disruption of neural activity in V1/V2 impaired the contour

detection performance was 120/140 ms after stimulus onset. The involvement of V1/V2 after V3B in representing contour-related information cannot be explained by the feed-forward model, which posits that V1, which represents simple features because of the smaller RF, is no longer required after the output of local feature computation feeding into higher visual areas, such as V4 (or V3B in the human brain). In contrast, our findings provided clear evidence that feedback processing is necessary to supplement feed-forward processing for complete contour integration.

The critical roles of feedback processing from higher to lower visual areas were extensively studied by using single/double-pulse TMS. These studies aimed to investigate the feedback from MT/V5 to early visual areas in motion perception (Pascual-Leone and Walsh 2001; Silvanto, Cowey et al. 2005; Silvanto, Lavie et al. 2005) and the feedback from lateral occipital (LO) area to early visual areas in the conscious experience of natural scene and perceptual completion (Koivisto et al. 2011; Wokke et al. 2013). However, causal evidence for recurrent interactions between V1 and V3B were much less understood. Our results suggested that TMS can be used to examine the processing dynamics of the important mid-level visual perception in the visual cortex.

Recent TMS studies have causally demonstrated that LO plays important roles in contour integration (Bona et al. 2014, 2015, 2016). Our results agree with these findings by demonstrating the importance of feedback sweep in contour integration. It is well known that the higher-level visual areas such as LO also play critical roles in higher-level processing such as object recognition. The relationship between contour integration and object recognition is a complex issue and beyond the scope of the present study. Nevertheless, the spatial-temporal dynamics between LO and early visual areas remains an interesting issue for further investigations.

Our results are consistent with the incremental grouping model for perceptual grouping that proposed an integrative framework of the feed-forward, feedback and horizontal connections in grouping image elements that belong to an object (Roelfsema 2006; Roelfsema and Houtkamp 2011). Specifically, the feed-forward sweep would generate a coarse template in higher visual areas with a larger RF, and the feedback interaction from the higher to lower visual areas contains the global information that can guide the computation of detailed local information. The neurons with smaller RF in the lower visual areas were suggested to complete the detailed computation with enhanced activity to the grouped contour elements relative to the background elements through horizontal connections. This model was supported by the neurophysiological data, which showed that the onset of the contour-related activity in V1 was later than that in V4 and these contour-related activities sustained during the processing of contour stimuli (Chen et al. 2014). The present study provides strong evidence that this model is implemented in the human brain. The undoubted role of feed-forward processing in contour integration is widely accepted because of the nature of V1 neurons in representing local features (e.g., orientation and spatial frequency). The earlier interference effect in V3B (i.e., 90/110 ms after stimulus onset) compared with V1/V2 suggested that the representation of contour began from the higher-level area after receiving the feed-forward input from V1/V2. The contour-related ERP components recorded from the human brain primarily occur at 150 ms after the stimulus onset (Pitts et al. 2012; Mijović et al. 2014; Volberg and Greenlee 2014). Therefore, we suggest that the observed early interference effect in V3B is related to the generation of a coarse template for the target contour. The coarse template was later sent back to V1, and this signal was related to the later interference effect due to V1/V2 stimulation. Moreover, at early stage of contour processing, the population neural responses in monkeys' V1 encode the individual elements of the contour and background, and the contour's popping out was accomplished with increased activity of the contour elements and suppressed activity of the background elements only at late stage of the process (Gilad et al. 2013, 2016). Computational analysis of the electrophysiological data further confirmed that this late process was realized through horizontal connections within V1 (Liang et al. 2017). The observed late but not early interference effect in V1 in our studies has provided causal evidence to support these proposals. Furthermore, given its necessity, the cycle of feed-forward, feedback and horizontal processing may repeat multiple times, and may constitute the recurrent mechanism suggested by the model (Roelfsema 2006; Chen et al. 2014). In our study, the significant interference effect at 120/140 ms SOA in V3B in Experiment 2 and the significant interference effects at 150/170 ms SOA in both V1/V2 and V3B in Experiment 1 well supported such repetitive nature of the recurrent mechanism.

The present results are also consistent with our previous behavioral findings that detection of contours, other than pure collinear, requires the involvement of top-down processing and access to conscious awareness (Li and Li 2015). The present study manipulated contour detection performance at an intermediate level of difficulty, which is closer to the imperfect natural environment. Our findings suggest an ecologically plausible mechanism in which the recurrent interaction between striate and extrastriate cortical areas plays a significant role for the detection of imperfect contours in a natural environment.

Supplementary Material

Supplementary data is available at *Cerebral Cortex* online.

Funding

References

Altmann CF, Bülthoff HH, Kourtzi Z. 2003. Perceptual organization of local elements into global shapes in the human visual cortex. Curr Biol. 13(4):342–349.

Alvarez IA, Haas B, Clark CA, Rees G, Schwarzkopf DS. 2015. Comparing different stimulus configurations for population receptive field mapping in human fMRI. Front Hum Neurosci. 9:96.

Angelucci A, Levitt JB, Walton EJS, Hupe J, Bullier J, Lund JS. 2002. Circuits for local and global signal integration in primary visual cortex. J Neurosci. 22:8633–8646.

Bardi L, Kanai R, Mapelli D, Walsh V. 2012. Direct current stimulation (tDCS) reveals parietal asymmetry in local/global and salience-based selection. Cortex. 49(3):850–860.

Bona S, Cattaneo Z, Silvanto J. 2015. The causal role of the occipital face area (OFA) and lateral occipital (LO) cortex in symmetry perception. J Neurosci. 35(2):731–738.

Bona S, Cattaneo Z, Silvanto J. 2016. Investigating the causal role of rOFA in holistic detection of mooney faces and objects: an fMRI-guided TMS study. Brain Stimul. 9(4): 594–600.

Bona S, Herbert A, Toneatto C, Silvanto J, Cattaneo Z. 2014. The causal role of the lateral occipital complex in visual mirror symmetry detection and grouping: an fMRI-guided TMS study. Cortex. 51:46–55.

Bosking WH, Zhang Y, Schofield B, Fitzpatrick D. 1997. Orientation selectivity and the arrangement of horizontal connections in tree shrew striate cortex. J Neurosci. 17(6): 2112–2127.

Brainard DH. 1997. The psychophysics toolbox. Spat Vis. 10: 433–436.

Brozzoli C, Ishihara M, Göbel SM, Salemme R, Rossetti Y, Farnè A. 2008. Touch perception reveals the dominance of spatial over digital representation of numbers. Proc Natl Acad Sci USA. 105(14):5644–5648.

Buracas GT, Boynton GM. 2002. Efficient design of event-related fMRI experiments using M-sequences. Neuroimage. 16: 801–813.

Chen M, Yan Y, Gong X, Gilbert CD, Liang H, Li W. 2014. Incremental integration of global contours through interplay between visual cortical areas. Neuron. 82(3):682–694.

Dale AM, Fischl B, Sereno MI. 1999. Cortical surface-based analysis: I. segmentation, surface reconstruction. Neuroimage. 1949:179–194.

de Haas B, Schwarzkopf DS, Anderson EJ, Rees G. 2014. Perceptual load affects spatial tuning of neuronal populations in human early visual cortex. Curr Biol. 24:R66–R67.

Drewes J, Goren G, Zhu W, Elder JH. 2016. Recurrent processing in the formation of shape percepts. J Neurosci. 36(1): 185–192.

Dumoulin SO, Wandell BA. 2008. Population receptive field estimates in human visual cortex. Neuroimage. 39:647–660.

Epshtein B, Lifshitz I, Ullman S. 2008. Image interpretation by a single bottom-up top-down cycle. Proc Natl Acad Sci USA. 105:14298–14303.

Field DJ, Hayes A, Hess RF. 1993. Contour integration by the human visual system: evidence for a local "association field". Vis Res. 33(2):173–193.

Fischl B, Sereno MI, Dale AM. 1999. Cortical surface-based analysis ii: inflation, flattening, and a surface-based coordinate system. Neuroimage. 9(9):195–207.

Foxe JJ, Simpson GV. 2002. Flow of activation from V1 to frontal cortex in humans. Exp Brain Res. 142(1):139–150.

Gilad A, Meirovithz E, Slovin H. 2013. Population responses to contour integration: early encoding of discrete elements and late perceptual grouping. Neuron. 78(2):389–402.

Gilad A, Oz R, Slovin H. 2016. Uncovering the spatial profile of contour integration from fixational saccades: evidence for widespread processing in V1. Cereb Cortex. 1–13.

Hess RF, Hayes A, Field DJ. 2003. Contour integration and cortical processing. Physiol Paris. 97:105–119.

Jehee JFM, Roelfsema PR, Deco G, Murre JMJ, Lamme VAF. 2007. Interactions between higher and lower visual areas improve shape selectivity of higher level neurons-explaining crowding phenomena. Brain Res. 1157(1):167–176.

Kapadia MK, Ito M, Gilbert CD, Westheimer G. 1995. Improvement in visual sensitivity by changes in local context: parallel studies in human observers and in V1 of alert monkeys. Neuron. 15:843–856.

Kleiner M, Brainard D, Pelli DG. 2007. What's new in psychtoolbox-3. Percept. 36(14):1–16.

Koivisto M, Railo H, Revonsuo A, Vanni S, Salminen-Vaparanta N. 2011. Recurrent processing in V1/V2 contributes to categorization of natural scenes. J Neurosci. 31(7):2488–2492.

Kourtzi Z, Tolias AS, Altmann CF, Augath M, Logothetis NK. 2003. Integration of local features into global shapes: monkey and human fMRI studies. Neuron. 37(2):333–346.

Kuai S, Li W, Yu C, Kourtzi Z. 2016. Contour integration over time: psychophysical and fMRI evidence. Cereb Cortex. 27 (5):3042–3051.

Lestou V, Mi J, Lam L, Humphreys K, Kourtzi Z, Humphreys GW. 2014. A dorsal visual route necessary for global form perception: evidence from neuropsychological fMRI. J Cogn Neurosci. 26(3):621–634.

Li S, Mayhew SD, Kourtzi Z. 2009. Learning shapes the representation of behavioral choice in the human brain. Neuron. 62 (3):441–452.

Li W, Gilbert CD, Piëch V. 2008. Learning to link visual contours. Neuron. 57:442–451.

Li W, Piëch V, Gilbert CD. 2006. Contour saliency in primary visual cortex. Neuron. 50:951–962.

Li Y, Li S. 2015. Contour integration, attentional cuing, and conscious awareness: An investigation on the processing of collinear and orthogonal contours. J Vis. 15:1–16.

Liang H, Gong X, Chen M, Yan Y, Li W, Gilbert CD. 2017. Interactions between feedback and lateral connections in the primary visual cortex. Proc Natl Acad Sci USA. 114(32): 8637–8642.

Mevorach C, Humphreys GW, Shalev L. 2006. Opposite biases in salience-based selection for the left and right posterior parietal cortex. Nat Neurosci. 9(6):740–742.

Mevorach C, Humphreys GW, Shalev L. 2009. Reflexive and preparatory selection and suppression of salient information in the right and left posterior parietal cortex. J Cogn Neurosci. 21(6):1204–1214.

Mijovi B, De Vos M, Vanderperren K, Machilsen B, Sunaert S, Van Huffel S, Wagemans J. 2014. The dynamics of contour integration: a simultaneous EEG-fMRI study. Neuroimage. 88:10–21.

Ostwald D, Lam JM, Li S, Kourtzi Z. 2008. Neural coding of global form in the human visual cortex. J Neurophysiol. 99: 2456–2469.

Pasalar S, Ro T, Beauchamp MS. 2010. TMS of posterior parietal cortex disrupts visual tactile multisensory integration. Eur J Neurosci. 31(10):1783–1790.

Pascualleone A, Walsh V. 2001. Fast backprojections from the motion to the primary visual area necessary for visual awareness. Science. 292(5516):510–512.

Pelli DG. 1997. The VideoToolbox software for visual psychophysics: transforming numbers into movies. Spat Vis. 10(4): 437–442.

Pitcher D, Goldhaber T, Duchaine B, Walsh V, Kanwisher NG. 2012. Two critical and functionally distinct stages of face and body perception. J Neurosci. 32(45):15877–15885.

Pitts MA, Martínez A, Hillyard SA. 2012. Visual processing of contour patterns under conditions of inattentional blindness. J Cogn Neurosci. 24(2):287–303.

Ramalingam N, McManus JNJ, Li W, Gilbert CD. 2013. Top-down modulation of lateral interactions in visual cortex. J Neurosci. 33(5):1773–1789.

Roelfsema PR. 2006. Cortical algorithms for perceptual grouping. Annu Rev Neurosci. 29:203–227.

Roelfsema PR, Houtkamp R. 2011. Incremental grouping of image elements in vision. Atten Percept Psychophys. 73(8): 2542–2572.

Salminen-Vaparanta N, Noreika V, Revonsuo A, Koivisto M, Vanni S. 2012. Is selective primary visual cortex stimulation achievable with TMS? Hum Brain Mapp. 33:652–665.

Schwarzkopf DS, Anderson EJ, de Haas B, White SJ, Rees G. 2014. Larger extrastriate population receptive fields in autism spectrum disorders. J Neurosci. 34(7):2713–2724.

Schwarzkopf DS, Zhang J, Kourtzi Z. 2009. Flexible learning of natural statistics in the human brain. J Neurophysiol. 102(3): 1854–1867.

Shpaner M, Molholm S, Forde E, Foxe JJ. 2013. Disambiguating the roles of area V1 and the lateral occipital complex (LOC) in contour integration. Neuroimage. 69:146–156.

Silvanto J, Cowey A, Lavie N, Walsh V. 2005. Striate cortex (V1) activity gates awareness of motion. Nat Neurosci. 8(2):143–144.

Silvanto J, Lavie N, Walsh V. 2005. Double dissociation of V1 and V5/MT activity in visual awareness. Cereb Cortex. 15 (11):1736–1741.

Stettler DD, Das A, Bennett J, Gilbert CD. 2002. Lateral connectivity and contextual interactions in macaque primary visual cortex. Neuron. 36:739–750.

Tootell RB, Hadjikhani N. 2001. Where is "dorsal V4" in human visual cortex? Retinotopic, topographic and functional evidence. Cereb Cortex. 11:298–311.

Tootell RBH, Tsao D, Vanduffel W. 2003. Neuroimaging weighs in: humans meet macaques in "primate" visual cortex. J Neurosci. 23(10):3981–3989.

Vanni S, Henriksson L, James AC. 2005. Multifocal fMRI mapping of visual cortical areas. Neuroimage. 27:95–105.

Volberg G, Greenlee MW. 2014. Brain networks supporting perceptual grouping and contour selection. Front Psychol. 5: 264.

Walsh V, Pascual-Leone A. 2003. Transcranial magnetic stimulation: a neurochronometrics of mind. Cambridge(MA): MIT Press.

Wandell BA, Dumoulin SO, Brewer AA. 2007. Visual Field Maps in Human Cortex. Neuron. 56(2):366–383.

Wandell BA, Winawer J. 2015. Computational neuroimaging and population receptive fields. Trends Cogn Sci. 19(6): 349–357.

Wokke ME, Vandenbroucke ARE, Scholte HS, Lamme VAF. 2013. Confuse your illusion: feedback to early visual cortex contributes to perceptual completion. Psychol Sci. 24:63–71.

Zhang J, Kourtzi Z. 2010. Learning-dependent plasticity with and without training in the human brain. Proc Natl Acad Sci USA. 107(30):13503–13508.